Quaternary Science Reviews 30 (2011) 1576–1582

Contents lists available at ScienceDirect

Quaternary Science Reviews

journal homepage: www.elsevier.com/locate/quascirev

Enhanced Atlantic Meridional Overturning Circulation supports the Last Glacial Inception

Abel Guihou [a,b,*], Sylvain Pichat [b], Aline Govin [a,1], Silvia Nave [c], Elisabeth Michel [a], Jean-Claude Duplessy [a], Philippe Telouk [b], Laurent Labeyrie [a]

[a] Laboratoire des Sciences du Climat et de l'Environnement/IPSL, CEA/CNRS/UVSQ, 91198 Gif sur Yvette, France
[b] Laboratoire de Géologie de Lyon, Ecole Normale Supérieure de Lyon et Université Claude Bernard, CNRS, 46 allée d'Italie, Lyon 69007, France
[c] Laboratório Nacional de Energia e Geologia, Unidade de Geologia Marinha, Lisboa, Portugal

ARTICLE INFO

Article history:
Received 17 November 2010
Received in revised form
17 March 2011
Accepted 29 March 2011
Available online 22 April 2011

Keywords:
Paleoceanography
AMOC
Glacial inception
Last Interglacial
231Pa/230Th

ABSTRACT

The Atlantic Meridional Overturning Circulation (AMOC) is a key feature of the climate system. However, its role during climate change is still poorly constrained particularly during an Interglacial to Glacial climate transition and the associated global cooling. We present here the first reconstruction of the evolution of the vertical structure of the rate of the AMOC from the Last Interglaciation to the subsequent glaciation (128,000–60,000 years ago) based on sedimentary (^{231}Pa/^{230}Th) records. We show a deep AMOC during the interglacial warmth Marine Isotope Stage (MIS) 5.5 and a shallower glacial one during glacial MIS 4. The change between these two patterns occurred mostly during the glacial inception, i.e. the transition from MIS 5.5 to MIS 5.4. Our data show that AMOC was enhanced during this latter transition as a consequence of a large increase of the overturning rate of the Intermediate Waters, above 2500 m. We suggest that this AMOC pattern required a reinforced Gulf Stream-North Atlantic Current system that ultimately supported ice-sheet growth by providing heat and moisture to the Northern high latitudes. From MIS 5.4 to MIS 5.1, the AMOC was broadly continuous below 2000 m and supported periods of ice-sheet growth. As a result, a glacial AMOC is triggered at the beginning of MIS 4 due to the extension of ice-sheet and the subsequent reorganization of deep-water formation. This study highlights the role of intermediate waters as a major player during climate change.

1. Introduction

The Atlantic Meridional Overturning Circulation (AMOC) is one of the most important ocean current system for the climate of the Earth, in particular because it controls the amount of northward heat transport in the northern hemisphere and the repartition of both water masses and chemical species, notably CO_2. Under modern conditions, the AMOC is composed of a surface current flowing northward from the tropics to the high latitudes, through the Gulf Stream and the North Atlantic Current, and a deep-water mass flowing southward: the North Atlantic Deep Water (NADW). At high latitudes, in the Nordic Seas and in the Labrador Sea, the warm and saline surface water, transported from the tropics, cools and loses buoyancy. These waters sink to form the NADW. Thus, the surface currents and the NADW are ultimately linked (Labeyrie et al., 1999). The AMOC is controlled by external and internal forcing mechanisms (Rahmstorf, 2002; Kuhlbrodt et al., 2007), e.g. insolation, freshwater flux, ice-sheet dynamics, vertical mixing in the ocean's interior and wind-induced Ekman upwelling in the Southern Ocean. However the sensitivity of the AMOC to these forcings remains elusive.

This study brings major constraints on the response of the AMOC to the forcing mechanisms by a detailed study of the Last Interglaciation and the subsequent glaciation (128,000 to 60,000 years ago). The Last Interglaciation was characterized by reduced ice volume at high Northern latitude during the warm Marine Isotope Stage (MIS) 5.5 (Koerner, 1989; de Vernal and Hillaire-Marcel, 2008) rapidly followed by ice-sheet growth in response to the climatic amplification of insolation forcing (Khodri et al., 2001; Waelbroeck et al., 2002; Wang and Mysak, 2002; Rohling et al., 2008). While numerous proxy data and model simulations

* Corresponding author. Present address: Lamont Doherty Earth Observatory of Columbia University, 61 Route 9W, Palisades, NY 10964-8000, USA. Tel.: +1 845 365 8653.
E-mail address: abel.guihou@gmail.com (A. Guihou).
[1] Present address: MARUM – Center for Marine Environmental Sciences, University of Bremen, Bremen, Germany.

0277-3791/$ – see front matter © 2011 Elsevier Ltd. All rights reserved.
doi:10.1016/j.quascirev.2011.03.017

are available for the transition from the warm optimum MIS 5.5 to the colder MIS 5.4, i.e. the glacial inception, there is little information covering the full transition up to glacial MIS 4. Moreover, studies aiming at understanding the AMOC response to the Last Glacial Inception are based on proxies which are indirectly linked to ocean circulation such as benthic foraminifera $\delta^{13}C$ (Duplessy et al., 1988) or foraminifera calcite Cd/Ca (Adkins et al., 1997) that mostly depict deep-water chemical properties. LeGrand and Wunsch (1995) showed that deep ocean circulation is indeed poorly constrained by such proxies, which are strongly affected by changes in biological productivity and in the carbon cycle.

In order to better constrain the processes at the origin of AMOC variability in response to climate change, we used a proxy – the sedimentary $^{231}Pa/^{230}Th$ excess activity ratio decay corrected to the time of deposition (hereafter referred to as ($^{231}Pa/^{230}Th$)) – that is more directly dependent on the rate of the AMOC. Both ^{231}Pa and ^{230}Th are produced in the water column by the radioactive decay of dissolved U with a constant production activity ratio of 0.093. The ($^{231}Pa/^{230}Th$) proxy is based on the difference between the residence time of the two radionuclides in the water column: ~200 years for ^{231}Pa and ~30 years for ^{230}Th (Yu et al., 1996; Francois, 2007). Under modern conditions, the residence time of ^{231}Pa in the water column is on the same order of magnitude as that of NADW in the North Atlantic. Therefore, ^{231}Pa can, in part, be exported out of the North Atlantic by deep-water circulation, while most of the ^{230}Th is scavenged locally to the sea floor by settling particles. Under modern conditions, the ($^{231}Pa/^{230}Th$) values above 2200 m water depth are around 0.093 (Yu et al., 1996; Hall et al., 2006; Gherardi et al., 2009) – the water column production ratio, whereas at greater depth ($^{231}Pa/^{230}Th$) are lower, typically around 0.05 (Yu et al., 1996; McManus et al., 2004; Gherardi et al., 2009), which indicates a large export of ^{231}Pa out of the North Atlantic by deep circulation. Due to the high affinity of ^{231}Pa for biogenic opal (Walter et al., 1997; Chase et al., 2002), changes in opal fluxes may complicate interpretation of ($^{231}Pa/^{230}Th$) records (Keigwin and Boyle, 2008; Gil et al., 2009; Lippold et al., 2009). So far, it is assumed that direct comparisons of biogenic opal fluxes with ($^{231}Pa/^{230}Th$) in the same samples are reliable indicators of the influence of biogenic opal fluxes changes on ($^{231}Pa/^{230}Th$) records (Francois et al., 1997; Bradtmiller et al., 2007). Following this approach, the ($^{231}Pa/^{230}Th$) has been successfully used to reconstruct AMOC variations for the Holocene, the Last Glacial Maximum (LGM) and the Last Deglaciation (Yu et al., 1996; McManus et al., 2004; Hall et al., 2006; Gherardi et al., 2009, 2010; Negre et al., 2010).

Guihou et al. (2010) have demonstrated that ($^{231}Pa/^{230}Th$) is suited to follow AMOC variations for deep-water masses (around 3500 m) during MIS 5 which expands the use of the ($^{231}Pa/^{230}Th$) proxy to its temporal limit at about 2–4 ^{231}Pa half-lives.

In order to investigate the response of the AMOC to the chain of events leading the establishment of the last glacial period, we present here new ($^{231}Pa/^{230}Th$) data from intermediate depth North Atlantic sediment cores coupled with published results from deep North Atlantic sites (Guihou et al., 2010) over the period 128,000–60,000 years ago. We studied past changes in the intermediate and deep AMOC by reconstructing the vertical structure of the rate of the AMOC for key intervals of the Last Interglaciation and the subsequent glaciation.

2. Materials and methods

In order to explore the variability of the ($^{231}Pa/^{230}Th$) with water depth and time, we studied a set of sediment cores located in the North Atlantic Ocean in a narrow latitudinal range between 37°N and 44°N (Fig. 1), a zone that is optimal to monitor changes in the rate of the AMOC as modeled by Siddall et al. (2007) and Luo et al. (2010). We have chosen cores located off the margins to avoid the effect of boundary scavenging on ($^{231}Pa/^{230}Th$) (Bacon, 1988). A common stratigraphy for the cores has been established based on conventional $\delta^{18}O$ correlation (Fig. 2).

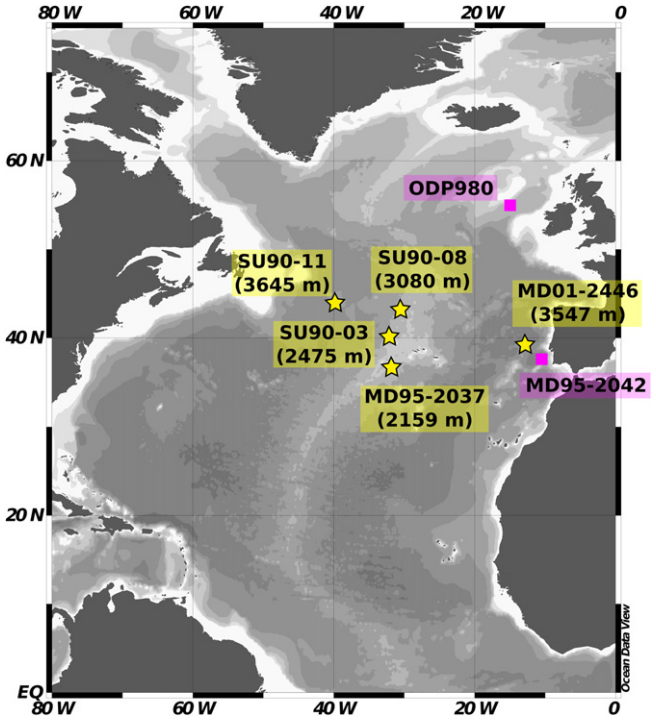

Fig. 1. Map showing the location of the cores used in this study. The stars show the location of the cores which were analysed for ($^{231}Pa/^{230}Th$): cores MD95-2037 (37.09°N, 32.04°W, 2159 m water depth) (this study), SU90-03 (40.07°N, 32.02°W, 2475 m water depth) (this study) and SU90-08 (42.05°N, 32.03°W, 3080 m water depth) (this study) on the slopes of the mid Atlantic Ridge; core MD01-2446 (39.05°N, 12.62°W, 3547 m water depth) (Guihou et al., 2010) off the Iberian Margin and core SU90-11 (44.07°N, 40.02°W, 3645 m water depth) (Guihou et al., 2010) from the western North Atlantic basin. The squares show the location of reference cores ODP980 (55.48°N, 14.70°W, 2168 m) and MD95-2042 (37.80°N, 10.17°W, 3146 m) used for latitudinal sea surface temperature (SST) gradient reconstructions (Fig. 5c). The map was generated with Ocean Data View (http://odv.awi.de/en/home/).

Pa, Th and U have been extracted from 200 mg of bulk sediment for each analysis. The analytical process was conducted following Guihou et al. (2010) in a class 10,000 clean laboratory at Laboratoire de Géologie de Lyon, France (LGL, ENS Lyon). Briefly, samples were spiked with ^{229}Th, ^{236}U and ^{233}Pa. The latter was obtained from the milking of a ^{237}Np mother solution. After sediment digestion and spike equilibration, Pa, Th and U were extracted from the matrix by iron oxyhydroxide precipitation at pH 8–10. Pa, Th and U were then separated by anion exchange chromatography using BioRad® AG1-x8 resin. Both Pa and Th fractions were further purified by anion exchange chromatography (BioRad® AG1-x8 resin). The Pa, Th and U fractions were measured by Multi-Collector Inductively Coupled Plasma Mass Spectrometer (MC-ICPMS Nu 500 HR, Nu Instrument®) using multi-ion counters on the French National Facility Instrument (INSU-CNRS) at the LGL, ENS Lyon. Each sample analysis was bracketed using the IRMM 184 isotopic uranium standard to correct for instrumental mass bias and ion-counters gain. Results were corrected for instrumental and chemistry background and then reduced to calculate excess fractions following Thomas et al. (2007). A detrital ($^{238}U/^{232}Th$) ratio of 0.5 ± 0.1 was used (Guihou et al., 2010). Uncertainties on the ($^{231}Pa/^{230}Th$) were calculated by error propagation assuming independent and normally distributed variables, they are typically about ±0.005 (1 SD).

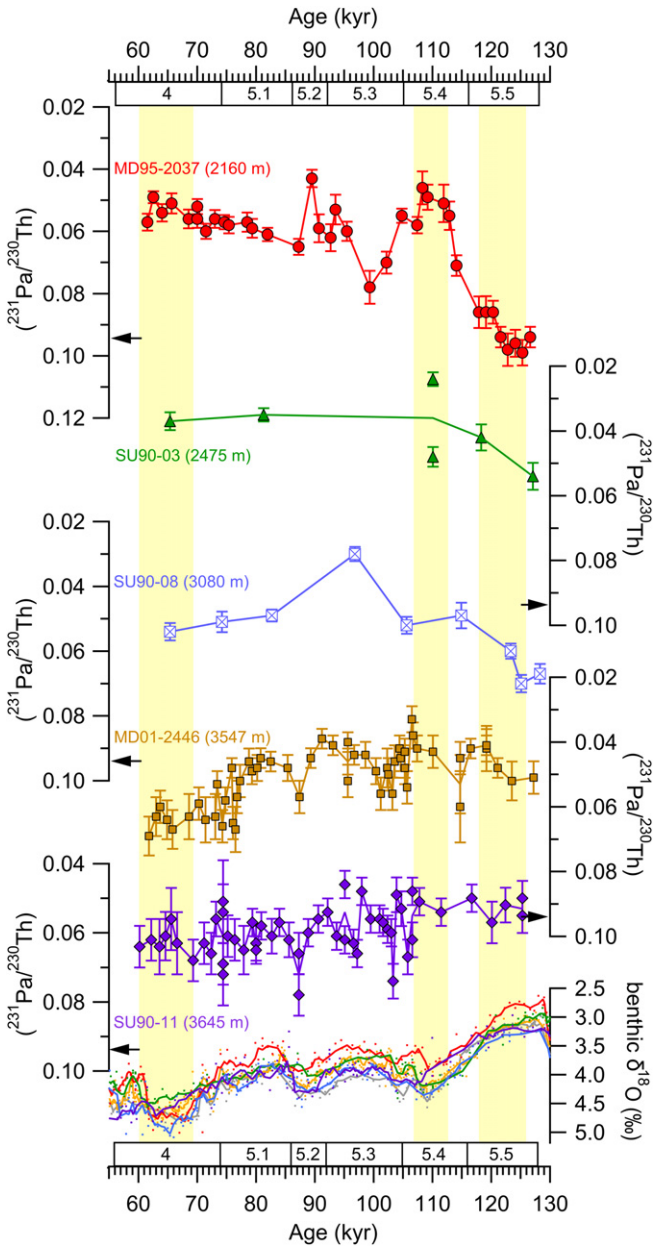

Fig. 2. (^{231}Pa/^{230}Th) records from the 5 cores considered in this study. (^{231}Pa/^{230}Th) data from Black arrows indicate the water column (^{231}Pa/^{230}Th) production ratio, i.e. 0.093. Error bars represent the propagated standard deviation (1 SD) (Guihou et al., 2010). Benthic (*C. wuellerstorfi*) δ^{18}O records of cores MD95-2037 (red dots), SU90-03 (green dots), SU90-08 (blue dots), SU90-11 (purple dots), MD95-2042 (orange dots) (Shackleton et al., 2003) and ODP980 (light grey dots) (Oppo et al., 2006) on the age scale derived from our stratigraphic framework. The curves are 3 point-running averages. The shaded areas represent the time periods emphasized in Section 3.2 (i.e. MIS 5.5 (126,000–118,000 years ago), MIS 5.4 (113,000–107,000 years ago) and MIS 4 (69,000–60,000 years ago)). Marine Isotope Stages are indicated at the top and the bottom of the figure. (For interpretation of the references to colour in this figure legend, the reader is referred to the web version of this article.)

3. Results and discussion

The amplitudes and trends of the (^{231}Pa/^{230}Th) downcore profiles differ with water depth (Fig. 2, Supplementary Material). The shallowest record displays the largest (^{231}Pa/^{230}Th) change at the transition from MIS 5.5 to MIS 5.4, from values close to 0.093 – the production ratio – to values around 0.045 while from MIS 5.4 to MIS 4 (^{231}Pa/^{230}Th) display only minor variations around 0.05. The (^{231}Pa/^{230}Th) records of the cores located at 2475 m and 3080 m exhibit the same general trends with the highest values during MIS 5.5 and lower values corresponding to MIS 5.4 and MIS 4. The (^{231}Pa/^{230}Th) records of the deepest cores (Guihou et al., 2010) exhibit a trend opposite to those of the shallower sites. Their (^{231}Pa/^{230}Th) values are close to 0.05 during MIS 5.5 and slightly increase towards MIS 4 to values close to 0.065.

3.1. Assessing the validity of the (^{231}Pa/^{230}Th) records as AMOC proxies

While (^{231}Pa/^{230}Th) has been successfully used to reconstruct AMOC variations ((Gherardi et al., 2009) and references therein) change in biogenic opal flux have been proposed as a candidate that could account for (^{231}Pa/^{230}Th) variability (Keigwin and Boyle, 2008; Gil et al., 2009; Lippold et al., 2009), as Pa has a high affinity for opal (Walter et al., 1997; Chase et al., 2002). To constrain the potential local effect of biogenic opal, we calculated the biogenic opal fluxes in the three highest resolution records by normalizing the biogenic opal content (Supplementary Material) – measured by molybdate-blue spectrophotometry (Mortlock and Froelich, 1989) – to the ^{230}Th flux (Francois et al., 2004). Additionally, abundance of siliceous microfossils (mainly diatoms) were analysed in 30 samples of core SU90-11. Both methods are described in details by Guihou et al. (2010). Although the biogenic opal flux may be underestimated due to dissolution before or during burial, silicoflagellates valves, which indicate good preservation of biogenic opal (Hurd and Aston, 1983; Romero et al., 2002), were counted in 13 samples of core SU90-11 (Fig. 3). There is no correlation between the amount of silicoflagellates valves and ^{230}Th-normalized opal flux (Fig. 3). Thus opal dissolution cannot account for the variations in the opal flux at the analysed core sections. For the remaining samples of core SU90-11 and in the other cores, we chose to focus on measuring the opal content because counting is (1) highly time/cost consuming and (2) not fully relevant for assessing the potential effect of biogenic opal on (^{231}Pa/^{230}Th) records (Guihou et al., 2010). The correlation between ^{230}Th-normalized opal flux and (^{231}Pa/^{230}Th) is poor for SU90-11 and negative, i.e. opposite to what is expected, for the two other cores (Fig. 3). These results show that the (^{231}Pa/^{230}Th) records are

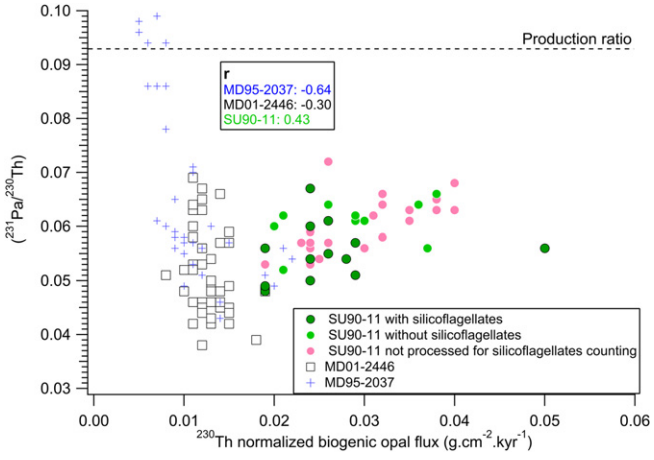

Fig. 3. Comparison of the biogenic opal flux (normalized to ^{230}Th) to the (^{231}Pa/^{230}Th) of core SU90-11 (circles) (Guihou et al., 2010), MD01-2446 (squares) (Guihou et al., 2010) and MD95-2037 (crosses). For core SU90-11, 30 samples were analysed for the abundance of siliceous microfossils, dark green means that silicoflagellates valves were present in the analysed samples while light green means that silicoflagellates valves were absent. For each core, the correlation coefficient (r) is shown. (For interpretation of the references to colour in this figure legend, the reader is referred to the web version of this article.)

not primarily controlled by local changes in biogenic opal flux. One could argue that remote changes in diatom productivity would affect the (^{231}Pa/^{230}Th). Indeed, a model by Luo et al. (2010) has shown that remote changes in opal flux can produce large changes in (^{231}Pa/^{230}Th) but also that these changes will be localized. Moreover, the (^{231}Pa/^{230}Th) records from cores SU90-11 (3645 m) and MD01-2446 (3547 m) are very similar (Fig. 2) although they are located in the western and eastern North Atlantic basins respectively and their biogenic opal flux differ (Fig. 3) (Guihou et al., 2010).

In the studied cores, local or remote variations in opal flux fail to explain the (^{231}Pa/^{230}Th) variations which can therefore be interpreted in terms of changes in the rate of the AMOC. Therefore, the three shallowest cores show generally increasing overturning rate from MIS 5.5 to MIS 4 while the two deepest cores, below 3500 m, show generally decreasing overturning rate over the same time period (Fig. 2).

3.2. Evolution of the vertical structure of the AMOC for specific time slices

In order to depict the vertical structure of the rate of the AMOC down to 3700 m during the Last Interglaciation and the subsequent glaciation, the (^{231}Pa/^{230}Th) record of each core was averaged over key time slices of this period of time: MIS 5.5 (126,000–118,000 years ago), MIS 5.4 (113,000–107,000 years ago) and MIS 4 (69,000–60,000 years ago) (Figs. 2 and 4).

3.2.1. AMOC vertical structure during MIS 5.5

During MIS 5.5, the overturning rate was high between 2200 m and 3600 m water depth and weak above 2200 m (Fig. 4a). The (^{231}Pa/^{230}Th) values recorded in this study for MIS 5.5 are remarkably similar to the values recorded for the Holocene (Fig. 4a). This AMOC structure is consistent with overturning of dense surface water in the Nordic seas (Duplessy et al., 2007) then flowing southward below 2200 m water depth. Hence during the warm optimum of MIS 5.5, the structure of the AMOC was similar to the Modern one.

3.2.2. AMOC vertical structure: glacial MIS 4

During the glacial MIS 4, the depth range where the overturning rate was the highest was centered around 2500 m whereas the overturning rate around 3500 m was lower than that of MIS 5.5 (Fig. 4b,c). This AMOC pattern is similar to the one of the LGM with (^{231}Pa/^{230}Th) values similar to the LGM ones (Fig. 4b). This pattern depicts a Glacial mode (Rahmstorf, 2002) for the AMOC for both MIS 4 and the LGM. We hypothesize that during MIS 4, deep-water formation did not occur in the Nordic Seas but mostly south of the Iceland-Scotland ridge as a consequence of the extension of the continental ice cover. Consequently, the Polar Front shifted southward due to changes in atmospheric circulation through the development of a polar vortex over the Greenland ice-sheet (Labeyrie et al., 1999). Thus, the extension of cold and low salinity surface waters in the Nordic Seas prevented their sinking to the abyss (Duplessy and Shackleton, 1985). The water mass, which sank south of the Scotland – Iceland ridge, was thus flowing around 2500 m and the pattern of AMOC during MIS 4 was dramatically different from that of MIS 5.5. Our study shows that there is a consistency between the vertical structure of the rate of the AMOC for the last two glacial maxima of the last climate cycle and points out the recurrence of two modes of ocean circulation associated with Interglacials and Glacials.

3.2.3. AMOC vertical structure: glacial inception (from MIS 5.5 to MIS 5.4)

A detailed analysis of the (^{231}Pa/^{230}Th) profile during MIS 5.4 (Fig. 4c) sheds light on the mechanisms involved into the transition between the interglacial and the glacial mode of ocean circulation. Around 3500 m water depth, the (^{231}Pa/^{230}Th) values of MIS 5.4 are similar to those of MIS 5.5 (Fig. 4c), indicating the presence of a deep overturning during both periods. Above 2500 m water depth, the (^{231}Pa/^{230}Th) values are significantly lower during MIS 5.4 than during MIS 5.5, with the largest magnitude of change occurring at 2200 m (Fig. 4c). Accordingly, the rate of overturning at

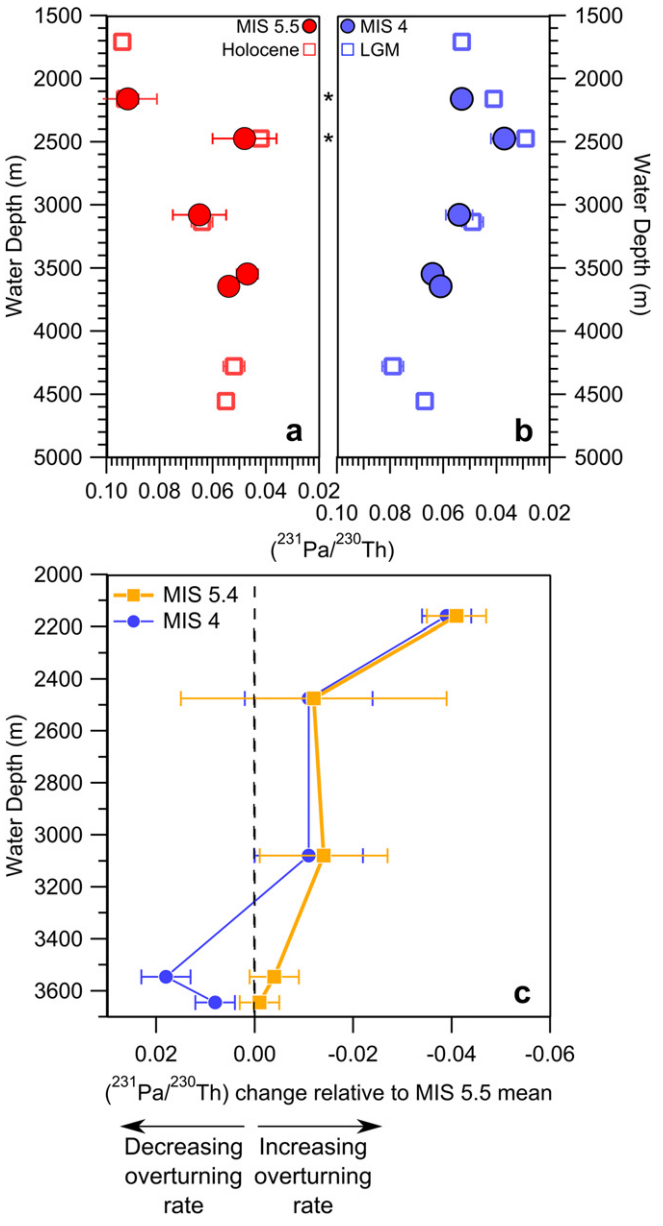

Fig. 4. Vertical profiles of the rate of the AMOC reconstructed over the Last Glacial Inception. (a.) Vertical profiles of averaged (^{231}Pa/^{230}Th) over MIS 5.5 (126,000 – 118,000 years ago; red circles) and the Holocene (red squares). (b.) Vertical profiles of averaged (^{231}Pa/^{230}Th) over MIS 4 (69,000 – 60,000 years ago; blue circles) and the Last Glacial Maximum (blue squares). Holocene and LGM data are from Jaccard et al. (2007) and Gherardi et al. (2009). The stars show the cores that were utilized both in this study for MIS 5.5 and 4 and in Jaccard et al. (2007) and Gherardi et al. (2009). Error bars are 2σ. (c.) (^{231}Pa/^{230}Th) changes of MIS 5.4 (period from 113,000 to 107,000 years ago, orange line and filled squares) and MIS 4 (blue dashed line and filled circles) relative to MIS 5.5. The value for MIS 5.4 of core SU90-08 has been calculated by averaging the two data points that bracket the period from 113,000 to 107,000 years ago. Error bars are 2σ. The vertical dashed line is the line of no change compared to MIS 5.5 average. (For interpretation of the references to colour in this figure legend, the reader is referred to the web version of this article.)

intermediate depth was higher during MIS 5.4 than during MIS 5.5. This view is supported by the model of Luo et al. (2010) showing that an increase in the overturning rate at intermediate depth result in a sharp decrease in (^{231}Pa/^{230}Th) at the corresponding depth, and a rapid attenuation of the signal below. The increase of the overturning rate around 2200 m started at 120,000 years ago, i.e. during MIS 5.5. It followed the decrease in Northern Hemisphere summer insolation which favoured the initiation of ice-sheet growth (Khodri et al., 2001) (Fig. 5a,b). Conversely, the overturning rate remained constant around 3500 m. Consequently, overturning of dense surface water must have occurred in the Nordic Seas during that period. This feature is consistent with high benthic δ^{13}C in the Norwegian Sea sediments (Labeyrie et al., 1987) due to inflow of warm, saline and ventilated waters along the Norwegian coast (Risebrobakken et al., 2007; Born et al., in press) which sank during winter. Bauch and Erlenkeuser (2008) have also shown that above the Vøring Plateau (located between the Norwegian Sea and the Norwegian coast) the end of MIS 5.5 is characterized by warm and saline surface waters.

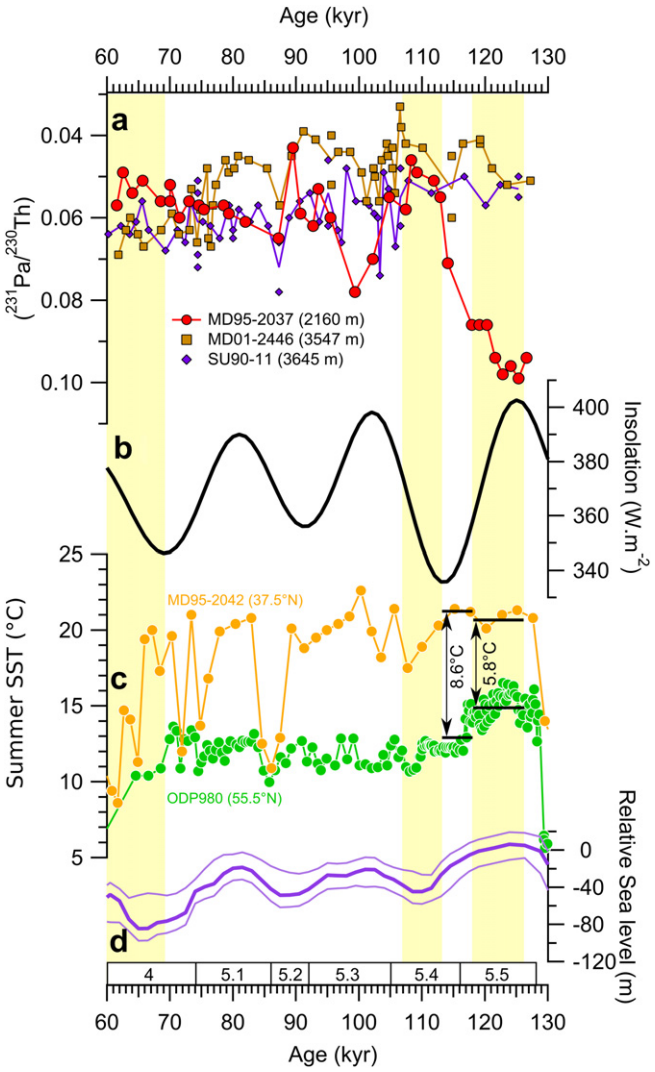

Fig. 5. Climate reconstruction from MIS 5.5 to MIS 4. (a.) (^{231}Pa/^{230}Th) of the three highest resolution cores, (b.) Summer insolation integrated from June 21st to September 21st at 65°N (Berger, 1978) (c.) MD95-2042 summer SST derived from foraminifera assemblages (Cayre et al., 1999) depicting SST changes at 37.5°N (orange line) and ODP980 (55.48°N, 14.70°W, 2168 m) summer SST derived from foraminifera assemblages (Oppo et al., 2006) depicting SST changes at high latitudes (green line). (d.) Sea level reconstruction relative to the modern one (Waelbroeck et al., 2002). The shaded areas are the time periods emphasized in Section 3.2. (For interpretation of the references to colour in this figure legend, the reader is referred to the web version of this article.)

Although our (^{231}Pa/^{230}Th) data show that the overturning rate remained globally unchanged around 3500 m between MIS 5.5 and MIS 5.4, the time-resolution is not as detailed as other paleoclimatic reconstructions. Indeed, high resolution SST reconstructions in the northeast Atlantic and in the Nordic Sea shows that the input of warm waters may not have been constant over that period as short term climate cooling phases have been evidenced (Fronval et al., 1998; Bauch and Kandiano, 2007). These events may have affected deep-water formation as suggested by increased Cd/Ca, a proxy for deep-water chemistry, that show that waters originating from the Southern Ocean were present at 4200 m in the Western North Atlantic (Adkins et al., 1997) in agreement with an early increase in Antarctic Bottom Water formation (Govin et al., 2009).

The continuity equation requires that the increase of Intermediate Water overturning rate together with constant overturning rate around 3500 m at the end of MIS 5.5 and during MIS 5.4 is balanced by an enhanced Gulf Stream-North Atlantic Current system. This strong Gulf Stream-North Atlantic Current system resulted from the increased latitudinal temperature gradient during the MIS 5.4 to MIS 5.5 transition (Fig. 5c). It carried heat and moisture from the tropics to the Northern high latitudes and thus contributed to feed ice-sheet growth over the Laurentide (Ruddiman and McIntyre, 1981) and Scandinavia (Baumann et al., 1995; Bonelli et al., 2009).

3.3. AMOC: from the end of MIS 5.4 to the beginning of MIS 4

After MIS 5.4 and up to the beginning of MIS 4, the (^{231}Pa/^{230}Th) values are well below the production ratio between 2000 m and 3500 m water depth with second order substage variations (Figs. 2 and 5a). Above 2200 m, the overturning rate was lower during MIS 5.3 and MIS 5.1 than during MIS 5.2 but the amplitude of these oscillations were smaller than that of the MIS 5.5/MIS 5.4 transition. In the two deepest cores, substages variations have also been recognized with higher overturning rate during MIS 5.3 and MIS 5.1 than during MIS 5.2. This substage variability has been ascribed to the dynamics of the ice-sheet and its effect on the formation of deep-water through changes in atmospheric and sea surface patterns (Guihou et al., 2010). However, the main pattern that emerges from our shallow and deep (^{231}Pa/^{230}Th) records with values well below the production ratio (Figs. 2 and 5a) is a broadly continuous AMOC below 2000 m during MIS 5.3, 5.2 and 5.1. By bringing moisture and heat to the northern high latitudes, this continuous overturning supported periods of ice-sheet growth which are shown by the variations of the sea level (Fig. 5d).

The vertical structure of the rate of the AMOC during MIS 4 is therefore a consequence of ice-sheet growth that is fuelled by a strong Gulf Stream-North Atlantic Current system. Ultimately, at the beginning of MIS 4, the extension of the ice-sheets caused the southward displacement of the polar front and prevented the penetration of warm and saline surface waters into the Nordic Seas. This new surface circulation mode did not any more permit deep-water formation in the Nordic Seas but favoured sinking of surface water in the Atlantic Ocean, south of Norwegian-Iceland-Greenland sill during winter. This resulted in an Intermediate Water circulation.

4. Conclusion

These results provide compelling evidence that the rate of the AMOC was enhanced during the Last Glacial Inception. While the Northern high latitudes cooled down as a response to the decrease in Northern summer insolation, the AMOC was enhanced by the

increase in the latitudinal temperature gradient. The AMOC transported heat and moisture to the Northern high latitudes feeding ice-sheet growth. The AMOC thus acted as a strong positive feedback to fuel ice-sheet growth during the glacial inception. This increase in the rate of the AMOC was controlled by changes in the overturning rate of Intermediate Waters, i.e. around 2000 m. This water mass appears to be sensitive to changes in continental ice cover through atmospheric and sea surface patterns. An improved understanding of the physical mechanisms that drive Intermediate Water formation in the North Atlantic should thus remain a high priority for future investigations.

Acknowledgments

We are grateful to the Institut Universitaire de France, CEA, CNRS, UVSQ, ENS Lyon and Université de Lyon for providing financial support to perform most of this study. This work was supported by the INSU-CNRS PNEDC program (ClimaPaTh) to LL and SP, INSU-CNRS ECLIPSEII program to SP and Past4Future to EM. Opal data and siliceous microfossil analyses were produced in the framework of the ESF-EUROCORES programme, 06-EuroMARC-FP-008; through FCT EUROMARC/0002/2007) and the Chamoc-Si project (GRICES/CNRS). We are grateful to Samuel Jaccard for providing unpublished (^{231}Pa/^{230}Th) data on core SU90-03. We are indebted to Georges Meyer (INSTN CEA Saclay) for allowing us access to a laboratory equipped for handling radioactive material and for his assistance with gamma counting. We are grateful to Emmanuelle Albalat and Chantal Douchet for their technical assistance in the clean laboratory, Pierre Deschamps for providing the HU-1 solution, Gulay Isguder for picking most of the foraminifera, Fabien Dewilde for performing oxygen and carbon isotopic analyses and Lélia Matos for the technical support for opal analyses on cores MD01-2446 and SU90-11. We would also like to acknowledge the crew of the research vessel Marion–Dufresne and the French Paul Emile Victor Institute (IPEV) (especially Yvon Balut) for collecting some of the cores studied here. Core MD01-2446 was taken in the framework of the European POP project (EVK-2000-00089).

Finally, we are grateful to Joerg Lippold, two anonymous reviewers and the editor for their comments that greatly improved this manuscript.

Appendix Supplementary material

Supplementary data related to this article can be found online at doi:10.1016/j.quascirev.2011.03.017.

References

Adkins, J.F., Boyle, E.A., Keigwin, L.D., Cortijo, E., 1997. Variability of the North Atlantic thermohaline circulation during the Last Interglacial period. Nature 390, 154–156.

Bacon, M.P., 1988. Tracers of chemical scavenging in the ocean: boundary effects and large-scale chemical fractionation. Philosophical Transactions of the Royal Society of London A325, 147–160.

Bauch, H.A., Erlenkeuser, H., 2008. A "critical" climatic evaluation of last interglacial (MIS 5e) records from the Norwegian Sea. Polar Research 27 (2), 135–151.

Bauch, H.A., Kandiano, E.S., 2007. Evidence for early warming and cooling in North Atlantic surface waters during the Last Interglacial. Paleoceanography 22, PA1201.

Baumann, K.-H., Lackschewitz, K.S., Mangerud, J., Spielhagen, R.F., Wolf-welling, T.C.W., Henrich, R.d., Kassens, H., 1995. Reflection of Scandinavian ice sheet fluctuations in Norwegian Sea sediments during the past 150,000 Years. Quaternary Research 43 (2), 185–197.

Berger, A.L., 1978. Long-term variations of daily insolation and Quaternary climatic changes. Journal of the Atmospheric Sciences 35 (12), 2362–2367.

Bonelli, S., Charbit, S., Kageyama, M., Woillez, M.N., Ramstein, G., Dumas, C., Quiquet, A., 2009. Investigating the evolution of major Northern Hemisphere ice sheets during the Last Glacial–Interglacial cycle. Climate of the Past 5 (3), 329–345.

Born, A., Nisancioglu, K.H., Risebrobakken, B. Late Eemian warming in the Nordic Seas as seen in proxy data and climate models. Paleoceanography, in press, doi: 10.1029/2010PA002027.

Bradtmiller, L.I., Anderson, R.F., Fleisher, M.Q., Burckle, L.H., 2007. Opal burial in the equatorial Atlantic Ocean over the last 30 ka: implications for glacial-interglacial changes in the ocean silicon cycle. Paleoceanography 22, PA4216.

Cayre, O., Lancelot, Y., Vincent, E., Hall, M.A., 1999. Paleoceanographic reconstructions from Planktonic foraminifera off the Iberian margin: temperature, salinity, and Heinrich events. Paleoceanography 14 (3), 384–396.

Chase, Z., Anderson, R.F., Fleisher, M.Q., Kubik, P.W., 2002. The influence of particle composition and particle flux on scavenging of Th, Pa and Be in the ocean. Earth and Planetary Science Letters 204, 215–229.

de Vernal, A., Hillaire-Marcel, C., 2008. Natural variability of Greenland climate, vegetation, and ice volume during the past million years. Science 320 (5883), 1622–1625.

Duplessy, J.-C., Shackleton, N.J., 1985. Response of global deep-water circulation to Earth's climatic change 135,000–107,000 years ago. Nature 316 (6028), 500–507.

Duplessy, J.C., Roche, D.M., Kageyama, M., 2007. The deep Ocean during the Last Interglacial period. Science 316, 89–91.

Duplessy, J.C., Shackleton, N.J., Fairbanks, R.G., Labeyrie, L., Oppo, D., Kallel, N., 1988. Deepwater Source variations during the last climatic cycle and their impact on the global deepwater circulation. Paleoceanography 3 (3), 343–360.

Francois, R., 2007. Paleoflux and Paleocirculation from Sediment ^{230}Th and ^{231}Pa/^{230}Th, Proxies in Late Cenozoic Paleoceanography. Elsevier, Amsterdam, pp. 681–716.

Francois, R., Altabet, M.A., Yu, E.F., Sigman, D.M., Bacon, M.P., Frank, M., Bohrmann, G., Bareille, G., Labeyrie, L.D., 1997. Contribution of Southern Ocean surface-water stratification to low atmospheric CO_2 concentrations during the last glacial period. Nature 389, 929–935.

Francois, R., Frank, M., Rutgers-van-der-Loeff, M.M., Bacon, M.P., 2004. ^{230}Th normalization: an essentiel tool for interpreting sedimentary fluxes during the late Quaternary. Paleoceanography 19, PA1018.

Fronval, T., Jansen, E., Haflidason, H., Sejrup, J.P., 1998. Variability in surface and deep water conditions in the Nordic seas during the Last Interglacial period. Quaternary Science Reviews 17 (9–10), 963–985.

Gherardi, J.M., Labeyrie, L., Nave, S., Francois, R., McManus, J.F., Cortijo, E., 2009. Glacial-interglacial circulation changes inferred from ^{231}Pa/^{230}Th sedimentary record in the North Atlantic region. Paleoceanography 24, PA2204.

Gherardi, J.M., Luo, Y., Francois, R., McManus, J.F., Allen, S.E., Labeyrie, L., 2010. Glacial-interglacial circulation changes inferred from ^{231}Pa/^{230}Th sedimentary record in the North Atlantic region. Paleoceanography 25 (2), PA2207. Reply to comment by S. Peacock on.

Gil, I.M., Keigwin, L.D., Abrantes, F.G., 2009. Deglacial diatom productivity and surface ocean properties over the Bermuda Rise, northeast Sargasso Sea. Paleoceanography 24 (4), PA4101.

Govin, A., Michel, E., Labeyrie, L., Waelbroeck, C., Dewilde, F., Jansen, E., 2009. Evidence for northward expansion of Antarctic bottom water mass in the Southern Ocean during the Last Glacial Inception. Paleoceanography 24, PA1202.

Guihou, A., Pichat, S., Nave, S., Govin, A., Labeyrie, L., Michel, E., Waelbroeck, C., 2010. Late slowdown of the Atlantic meridional overturning circulation during the last glacial inception: new constraints from sedimentary (^{231}Pa/^{230}Th). Earth and Planetary Science Letters 289 (3–4), 520–529.

Hall, I.R., Moran, S.B., Zahn, R., Knutz, P.C., Shen, C.C., Edwards, R.L., 2006. Accelerated drawdown of meridional overturning in the late-glacial Atlantic triggered by transient pre-H event freshwater perturbation. Geophysical Research Letters 33, L16616.

Hurd, D.C., Aston, S.R., 1983. Physical and chemical properties of siliceous skeletons. Silicon Geochemistry and Biogeochemistry., 187–244.

Jaccard, S.L., Francois, R., Soon, M. and Labeyrie, L., 2007. Evidence from the central Atlantic for variability in the rate of intermediate- and deep water circulation over the past 50 kyrs., International Conference on Paleoceanography, Shanghai, China.

Keigwin, L.D., Boyle, E.A., 2008. Did North Atlantic overturning halt 17,000 years ago? Paleoceanography 23, PA1101.

Khodri, M., Leclainche, Y., Ramstein, G., Braconnot, P., Marti, O., Cortijo, E., 2001. Simulating the amplification of orbital forcing by ocean feedbacks in the last glaciation. Nature 410, 570–574.

Koerner, R.M., 1989. Ice core evidence for extensive melting of the Greenland ice sheet in the Last Interglacial. Science 244 (4907), 964–968.

Kuhlbrodt, T., Griesel, A., Montoya, M., Levermann, A., Hofmann, M., Rahmstorf, S., 2007. On the driving processes of the Atlantic meridional overturning circulation. Reviews of Geophysics 45, G2001.

Labeyrie, L., Leclaire, H., Waelbroeck, C., Cortijo, E., Duplessy, J.C., Vidal, L., Elliot, M., Le-Coat, B., Auffret, G., 1999. Temporal Variability of the Surface and Deep Waters of the North West Atlantic Ocean at Orbital and Millenial Scales. In: Geophysical Monograph 112. American Geophysical Union, pp. 77–98.

Labeyrie, L.D., Duplessy, J.C., Blanc, P.L., 1987. Variations in mode of formation and temperature of oceanic deep waters over the past 125,000 years. Nature 327 (6122), 477–482.

LeGrand, P., Wunsch, C., 1995. Constraints from Paleotracer data on the North Atlantic circulation during the Last Glacial Maximum. Paleoceanography 10 (6), 1011–1045.

Lippold, J., Grützner, J., Winter, D., Lahaye, Y., Mangini, A., Christl, M., 2009. Does sedimentary ^{231}Pa/^{230}Th from the Bermuda rise monitor past Atlantic meridional overturning circulation? Geophysical Research Letters 36, L12601.

Luo, Y., Francois, R., Allen, S.E., 2010. Sediment $^{231}Pa/^{230}Th$ as a recorder of the rate of the Atlantic meridional overturning circulation: insights from a 2-D model. Ocean Science 6 (1), 381–400.

McManus, J.F., Francois, R., Gherardi, J.M., Keigwin, L.D., Brown-Leger, S., 2004. Collapse and rapid resumption of Atlantic meridional overturning circulation linked to deglacial climate. Nature 428, 834–837.

Mortlock, R.A., Froelich, P.N., 1989. A simple method for the rapid determination of biogenic opal in pelagic marine sediments. Deep-Sea Research 36, 1415–1426.

Negre, C., Zahn, R., Thomas, A.L., Masque, P., Henderson, G.M., Martinez-Mendez, G., Hall, I.R., Mas, J.L., 2010. Reversed flow of Atlantic deep water during the Last Glacial Maximum. Nature 468 (7320), 84–88.

Oppo, D.W., McManus, J.F., Cullen, J.L., 2006. Evolution and demise of the Last Interglacial warmth in the subpolar North Atlantic. Quaternary Science Reviews 25 (23–24), 3268–3277.

Rahmstorf, S., 2002. Ocean circulation and climate during the past 120,000 years. Nature 419, 207–214.

Risebrobakken, B., Dokken, T., Ottera, O.H., Jansen, E., Gao, Y., Drange, H., 2007. Inception of the Northern European ice sheet due to contrasting ocean and insolation forcing. Quaternary Research 67, 128–135.

Rohling, E.J., Grant, K., Hemleben, C., Siddall, M., Hoogakker, B.A.A., Bolshaw, M., Kucera, M., 2008. High rates of sea-level rise during the Last Interglacial period. Nature Geoscience 1 (1), 38–42.

Romero, O.E., Lange, C.B., Wefer, G., 2002. Interannual variability (1988–1991) of siliceous phytoplankton fluxes off northwest Africa. Journal of Plankton Research 24 (10), 1035–1046.

Ruddiman, W.F., McIntyre, A., 1981. Oceanic mechanisms for amplification of the 23,000-year ice-volume cycle. Science 212 (4495), 617–627.

Shackleton, N.J., Sánchez-Goñi, M.F., Pailler, D., Lancelot, Y., 2003. Marine Isotope substage 5e and the Eemian Interglacial. Global and Planetary Change 36 (3), 151–155.

Siddall, M., Stocker, T.F., Henderson, G.M., Joos, F., Frank, M., Edwards, N.R., Ritz, S.P., Müller, S.A., 2007. Modeling the relationship between $^{231}Pa/^{230}Th$ distribution in North Atlantic sediment and Atlantic meridional overturning circulation. Paleoceanography 22, PA2214.

Thomas, A.L., Henderson, G.M., McCave, I.N., 2007. Constant bottom water flow into the Indian Ocean for the past 140 ka indicated by sediment $^{231}Pa/^{230}Th$ ratios. Paleoceanography 22, PA4210.

Waelbroeck, C., Labeyrie, L., Michel, E., Duplessy, J.C., McManus, J.F., Lambeck, K., Balbon, E., Labracherie, M., 2002. Sea-level and deep water temperature changes derived from benthic foraminifera isotopic records. Quaternary Science Reviews 21 (1–3), 295–305.

Walter, H.J., Rutgers van der Loeff, M.M., Hoeltzen, H., 1997. Enhanced scavenging of ^{231}Pa relative to ^{230}Th in the South Atlantic south of the Polar Front: implications for the use of the $^{231}Pa/^{230}Th$ ratio as a paleoproductivity proxy. Earth and Planetary Science Letters 149 (1–4), 85–100.

Wang, Z., Mysak, L.A., 2002. Simulation of the last glacial inception and rapid ice sheet growth in the McGill Paleoclimate Model. Geophysical Research Letters 29 (23), 2102.

Yu, E.F., Francois, R., Bacon, M.P., 1996. Similar rates of modern and last-glacial ocean thermohaline circulation inferred from radiochemical data. Nature 379, 689–694.